

Supporting Information

Copper Tungstate Photoanodes with Enhanced Solar Water Splitting Performance

*Kanishk Arunraj¹, Michael Wilms¹, Owen Kendall¹, Mitchell Perrin¹, Triet T. H. Nguyen¹,
Xiaoning Li¹, Peter C. Sherrell¹, Joel van Embden¹, Daniel E. Gómez¹, Rowena Yew²,
Noel Duffy², Enrico Della Gaspera^{1,*}*

¹ School of Science, RMIT University, Melbourne VIC 3000, Australia.

² CSIRO Energy, Clayton South, Victoria 3169, Australia

Corresponding author: *enrico.dellagaspera@rmit.edu.au

Experimental Methods

Solution synthesis and film deposition

A 0.1M solution of Copper (II) chloride (CuCl_2 , 99%, Sigma-Aldrich), ammonium metatungstate hydrate ($(\text{NH}_4)_6\text{H}_2\text{W}_{12}\text{O}_{40}\cdot x\text{H}_2\text{O}$, 99.99%, Sigma-Aldrich), and citric acid ($\text{C}_6\text{H}_8\text{O}_7$, 99%, Sigma-Aldrich) was prepared in a solvent mixture of N,N-dimethylformamide (DMF) and Milli-Q water. The volume ratio of DMF to water was maintained at 95:5. The chemicals were added sequentially to the solvent mixture and stirred at room temperature for 1 hour to ensure complete dissolution.

FTO-coated glass substrates (NSG TEC7, $\sim 7 \Omega/\square$) were cut into 1.5 cm \times 2.5 cm pieces, cleaned with soap and sponge, and rinsed with distilled water. Finally, the FTO substrates were ultrasonicated in Milli-Q water, ethanol, acetone and isopropyl alcohol (IPA) for 10 minutes each. The precursor solution was deposited on cleaned FTO glass substrates via spin coating: 60 μL of the precursor solution was dispensed onto the substrate, and the sample was spun at 3000 rpm for 30 seconds with immediate drying at 300 $^\circ\text{C}$ on a hotplate for 5 minutes after each coating step. The process was repeated to achieve the desired film thickness. The films were then annealed in a muffle furnace at various temperatures (400, 450, 500, 550 and 600 $^\circ\text{C}$) for 2 hours in ambient air. The samples were inserted in the furnace at ambient conditions, and the temperature was ramped at a rate of 8 $^\circ\text{C}/\text{min}$ up to the desired value. Selected samples were subjected to post-annealing in a tube furnace under a forming gas environment (4% hydrogen in argon) at various temperatures (100 – 300 $^\circ\text{C}$) for 2 hours.

FeNiOOH OER surface cocatalyst was deposited through electrodeposition adapted from a published recipe.¹ The deposition was conducted in a three-electrode photoelectrochemical (PEC) cell, with the CuWO_4 films as the working electrode, a platinum wire as the counter electrode, and an Ag/AgCl electrode as the reference. The electrolyte solution was prepared by dissolving 5 mM FeCl_3 , 3 mM NiCl_2 , 5 mM NaF, 0.1 M KCl and 1 M H_2O_2 in Milli-Q water. Cyclic voltammetry was performed using an electrochemical workstation (Metrohm Autolab PGSTAT204 potentiostat coupled with FRA32 impedance analyzer) to deposit the FeNiOOH cocatalyst on the CuWO_4 film surface. The potential was cycled between -0.49 and 0.41 V vs Ag/AgCl at a scan rate of 0.2 V/s for three cycles. Following deposition, the films were thoroughly rinsed with milli-Q water and air-dried.

Characterization techniques

X-ray diffraction (XRD) was conducted using a Bruker D4 Endeavor diffractometer equipped with a Cu-K α x-ray source operating at 40 kV and 35 mA. Crystallite size was estimated employing the Debye-Scherrer relationship using the full-width at half-maximum (FWHM) of the main peaks fitted using a Lorentzian function. Optical absorption spectroscopy of films deposited on FTO substrates was conducted using an Agilent Cary 5000 UV-Vis-NIR spectrophotometer equipped with an integrating sphere. Scanning Electron Microscopy (SEM) images were taken using FEI Verios 460L XHR-SEM. Energy dispersive x-ray (EDX) spectra and maps were acquired on the same microscope. X-ray photoelectron spectroscopy (XPS) was carried out using a Kratos Axis Supra XPS equipped with a monochromated Al K α X-ray source ($E_{\text{photon}} = 1486.7\text{eV}$) and a concentric hemispheric electron analyser. NMR spectroscopy was performed in ambient conditions using a Bruker Avance spectrometer (300 MHz) in DMF- d_7 (≥ 99.5 atom % D, Sigma-Aldrich). The X-ray absorption (XAS) spectra of the Cu K-edge were collected at the X-ray Spectroscopy Beamline (mode 1) at the Australian Synchrotron (AS, Australia). Raman spectroscopy was performed using a WiTEC Raman spectrometer via ControlFIVE software, and analyzed using the ProjectFIVE software. Spectra were obtained using a 532 nm laser with a 600 lines/mm grating through a 50x objective.

Photoelectrochemical (PEC) measurements were conducted using Metrohm Autolab PGSTAT204 potentiostat coupled with FRA32 impedance analyzer module using a 3-electrode configuration. CuWO $_4$ films on FTO were used as working electrode and mounted on a custom-made PEC cell, illuminated from the back using AM1.5G simulated sunlight. The aperture of the PEC cell defined the active area (0.45 cm 2). A Pt wire and an Ag|AgCl electrode were used as counter and reference electrode, respectively, and 0.1 M potassium phosphate (KPi) was used as electrolyte.

The PEC performance was measured using Linear Sweep Voltammetry (LSV) with scanning rate of 10 mV/s. The applied potential versus Ag|AgCl reference electrode (V_{AgCl}) was converted to Reversible Hydrogen Electrode (V_{RHE}) according to the following equation:

$$V_{\text{RHE}} = V_{\text{Ag|AgCl}} + V_{\text{Ag|AgCl vs RHE}}^{\circ} + 0.059 \cdot \text{pH} \quad (4)$$

where $V_{\text{Ag|AgCl}}^{\circ}$ is 0.197 V at 25 °C.

Selected electrochemical measurements were conducted using the same setup and acquisition parameters (10 mV/s, one data point every second), but using a blue LED as the

light source (455 nm, M455L3, Thorlabs), under pulsed conditions set by an automated LED driver (DC2200, Thorlabs) using a power density of 25 mW/cm², as measured by a photodiode power sensor (S120VC, Thorlabs).

Electrochemical Impedance Spectroscopy (EIS) was measured in 0.1 M KPi under simulated solar illumination at 1.23 V_{RHE} using AC voltage with amplitude of 10 mV RMS and frequency range of 100 kHz – 10 mHz. An appropriate equivalent circuit was fitted for all Nyquist plots using Metrohm Nova software to extract resistances.

The incident-photon-to-current conversion efficiency (IPCE) measurements were performed under irradiation from a Newport Xe lamp coupled to an Oriel Cornerstone 1/8 m adjustable slit monochromator, in a three-electrode cell containing 0.1 M KPi solution. A long-pass filter was placed in front of the monochromator to filter out higher-order diffracted light.

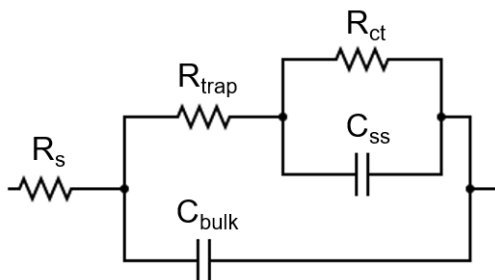
IPCE data was recorded at 1.23 V_{RHE} over a wavelength range of 310 to 810 nm, with a step size of 20 nm. IPCE was calculated using the following equation:

$$IPCE(\%) = \frac{1240 (V \times nm) \times j_{photo} \left(\frac{mA}{cm^2} \right)}{P_{mono} \left(\frac{mW}{cm^2} \right) \times \lambda (nm)} \times 100\%$$

where 1240 V × nm is the product of Planck's constant and the speed of light, j_{photo} is the measured photocurrent density in mA/cm², P_{mono} is the measured illumination power intensity in mW/cm² and λ (nm) is the wavelength at which this illumination power was measured. The illumination power intensity was measured using a Thorlabs PM100D power meter and a standard silicon photodiode power sensor with a wavelength range of 200–1100 nm.

Modelling of Electrochemical Impedance Spectroscopy data

We adopted the equivalent circuit proposed separately by Bartlett and Hamman for CuWO_4 and Fe_2O_3 , respectively (see image below).^{2,3}



In this circuit, R_s represents the overall series resistance which includes the bulk resistance of the semiconductor, the electrical contacts, and electrolyte. R_{trap} refers to the resistance associated with holes trapped in surface states. C_{bulk} represents the bulk capacitance, primarily dominated by space charge capacitance in the potential range used here. C_{ss} is the capacitance associated with surface states, and R_{ct} represents the charge transfer resistance at the surface. In other words, C_{bulk} captures the intrinsic capacitance linked to the materials space charge region, whilst C_{ss} and R_{ct} describe the interface-specific phenomena, such as trap-state-induced capacitance and resistance that govern charge transfer kinetics at the electrode/electrolyte interface. This equivalent circuit has been successfully used to model CuWO_4 EIS spectra, and to explain the role of surface states in the water oxidation activity of copper tungstate.

Figure S1

Raman spectra of a typical CuWO_4 film taken in two nominally identical areas. For one of them, the Raman signal shows a shoulder at $\sim 806 \text{ cm}^{-1}$ ascribed to WO_3 .

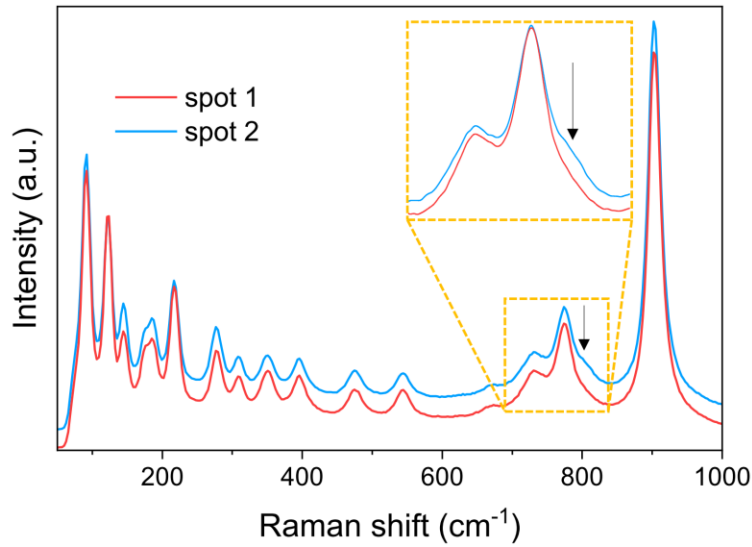


Figure S2

XPS analysis of a typical CuWO_4 film in the Cu 2p, W 4f and O 1s regions. The expected peak positions for Cu(II) and W(VI) are highlighted by vertical dashed lines.

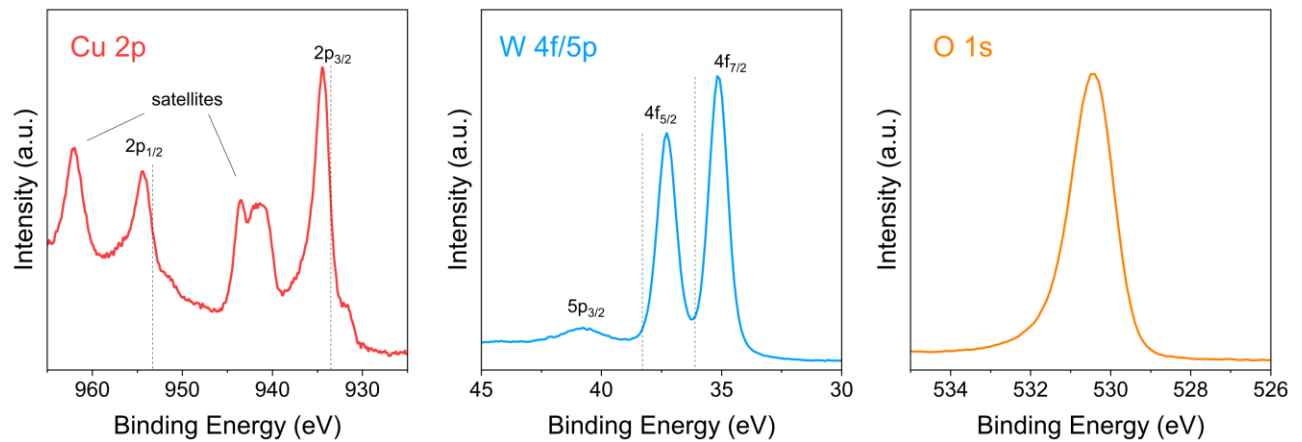


Figure S3

Normalized full X-ray absorption spectra (XAS) at the Cu K-edge for as-prepared CuWO_4 , CuO reference and Cu foil standard. The inset shows the corresponding normalized X-ray absorption near-edge structure (XANES) spectra. The edge position, typically defined at $\mu(E) = 0.65\text{-}0.75$, is used to estimate the oxidation state of the target element, indicating that the valence state of Cu follows the order $\text{CuWO}_4 > \text{CuO} > \text{Cu}$.

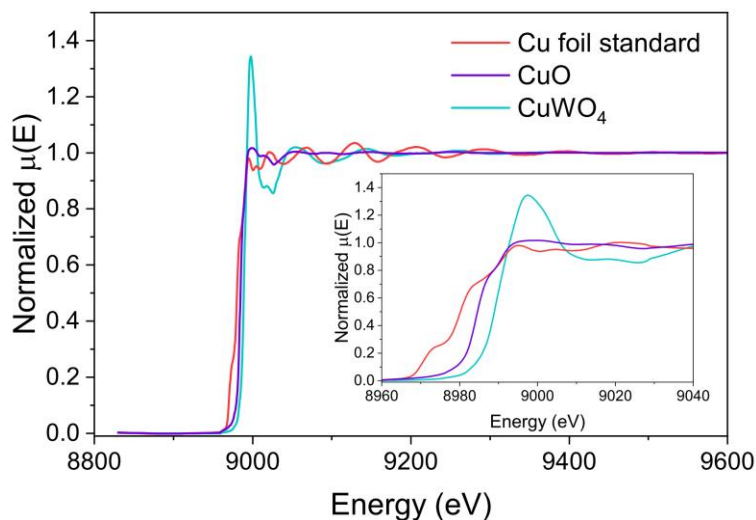


Figure S4

LSV curves for CuWO_4 samples prepared from precursor solutions with different combinations of water and DMF.

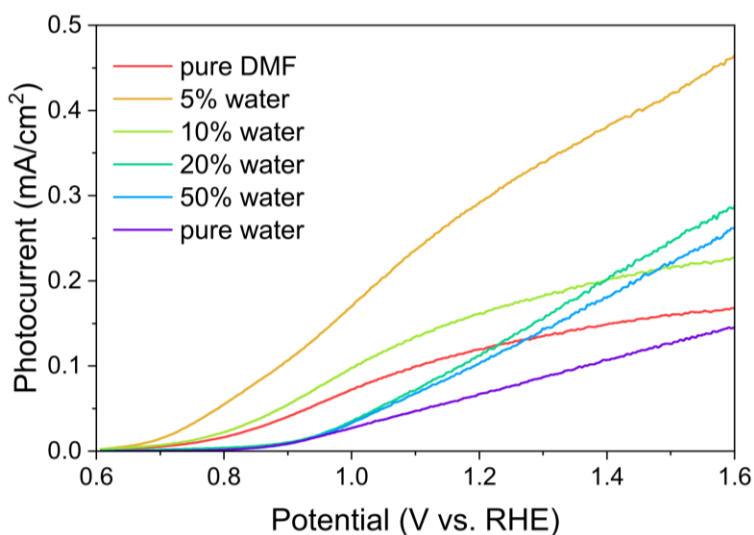


Figure S5

XRD patterns for CuWO_4 samples synthesized from DMF-based solutions with and without water as co-solvent. Only minor differences in the relative intensity of the diffraction peak can be observed.

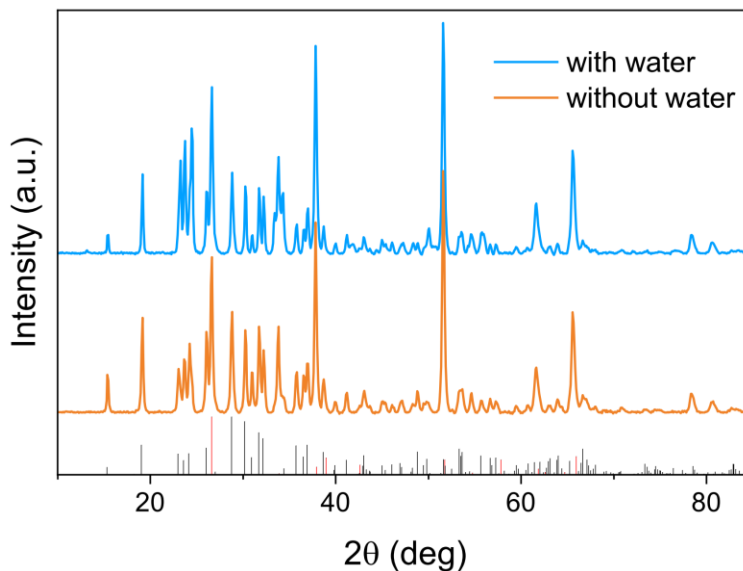


Figure S6

Raman spectra for CuWO_4 samples synthesized from DMF-based solutions with and without water as co-solvent. Clear signatures of WO_3 (highlighted by arrows) can be seen in the sample prepared without water.

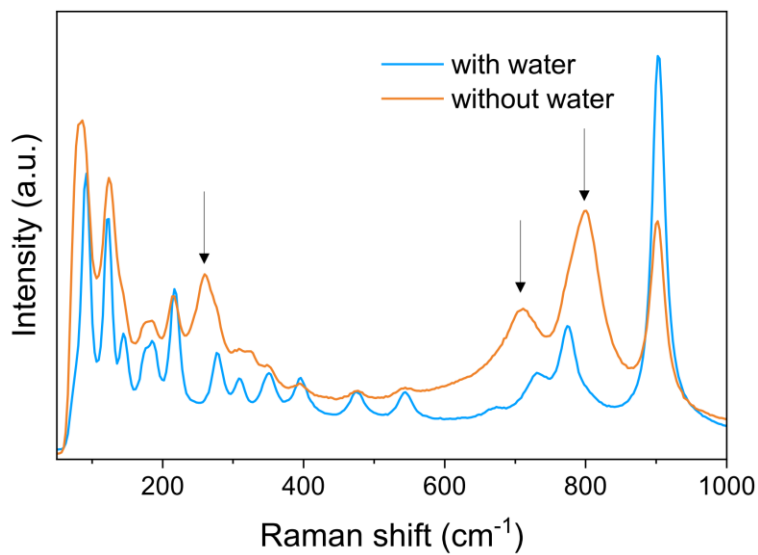


Figure S7

SEM images for CuWO_4 samples synthesized from DMF-based solutions with (5%) and without water as co-solvent. Clear morphological differences can be observed.

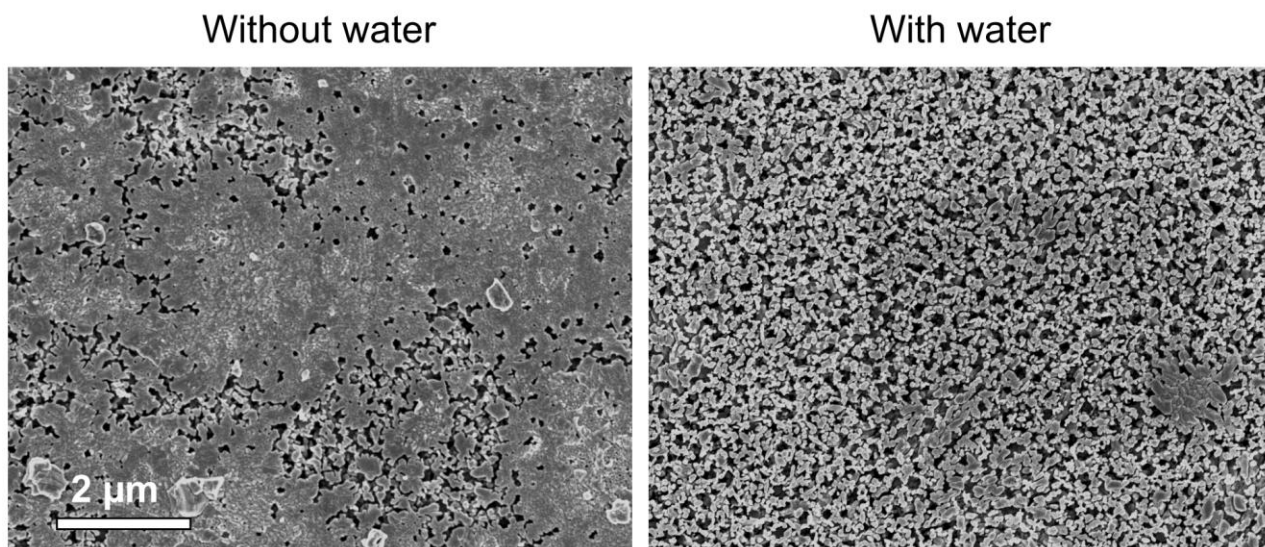
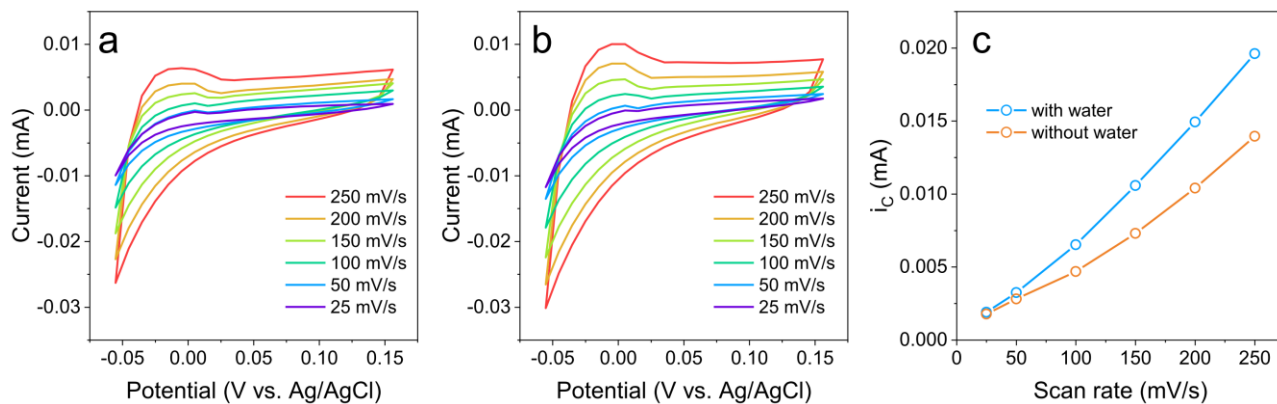


Figure S8

a,b) Cyclic voltammetry (CV) for CuWO_4 samples synthesized from DMF-based solutions without water (a) and with 5% water (b) as co-solvent. c) Relationship between current and scan rate at 0.05 V vs. Ag/AgCl. The slope of these curves is the double layer capacitance.



The electrochemically active surface area (EASA) can be calculated from the electrochemical double layer capacitance (C_{DL}). C_{DL} was calculated via cyclic voltammetry (CV) using the equation:

$$i_c = C_{DL} \times v$$

Here i_c represents the difference between the anodic (j_a) and cathodic (j_c) current at a given potential and v is the scan rate in mV/s. The C_{DL} of the samples were obtained from CV measurements conducted at varying scan rates within a potential window free of noticeable Faradaic reactions. Anodic and cathodic currents were taken at a specific potential (we chose 0.05 V vs. Ag/AgCl) and i_c was plotted against the scan rate. The slope of this curve corresponds to the C_{DL} . Although the trend is not perfectly linear, if we consider the range 50-250 mV, we obtained a reasonable fit ($R^2 > 0.98$ for both samples). The sample fabricated from water-containing solution exhibits a higher C_{DL} value ($\sim 39 \mu\text{F}/\text{cm}^2$) compared to the sample prepared without water ($\sim 27 \mu\text{F}/\text{cm}^2$). The EASA can be expressed as:

$$\text{EASA} = C_{DL}/C_s$$

where C_s is the capacitance for a perfectly planar and dense CuWO_4 . We could not determine the actual EASA values for these samples due to the inability to find a reliable value for the specific capacitance of CuWO_4 . However, regardless of the exact value of C_s , the EASA is directly proportional to the C_{DL} , and as such the ratio between the C_{DL} values of the two samples is equal to the ratio of the two EASA values. We can then conclude that the sample deposited from water-containing solution has higher EASA (roughly 40% higher) than the sample deposited from pure DMF.

Figure S9

EDS maps for CuWO_4 samples synthesized from DMF-based solutions without (top row) and with (bottom row) water as co-solvent. The scale bars are $1\ \mu\text{m}$. No major compositional differences could be detected, and the Cu:W atomic ratio is 1:1 (within experimental error) in both cases.

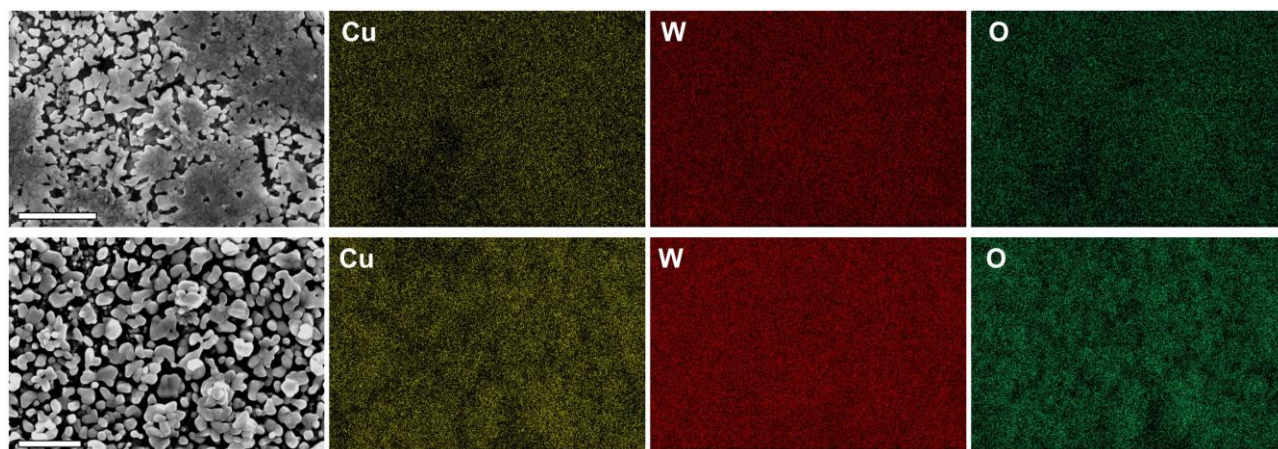


Figure S10

Photoelectrochemical performance evaluated as the photocurrent recorded at $1.23\ \text{V}$ vs. RHE, as a function of the thickness of the CuWO_4 photoanode produced from precursor solutions containing 5% water. A thickness of $\sim 1\ \mu\text{m}$ was found to be optimal for water oxidation.

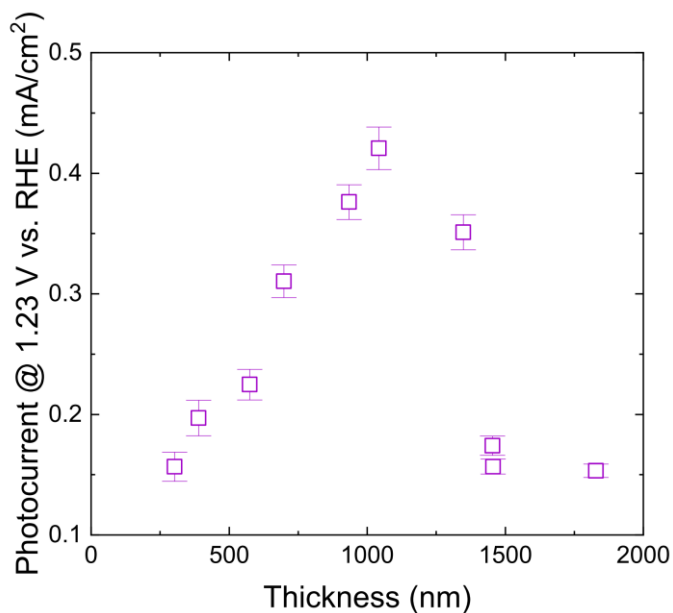


Figure S11

Reproducibility tests for 5 nominally identical CuWO_4 samples prepared from different precursor solutions in different days.

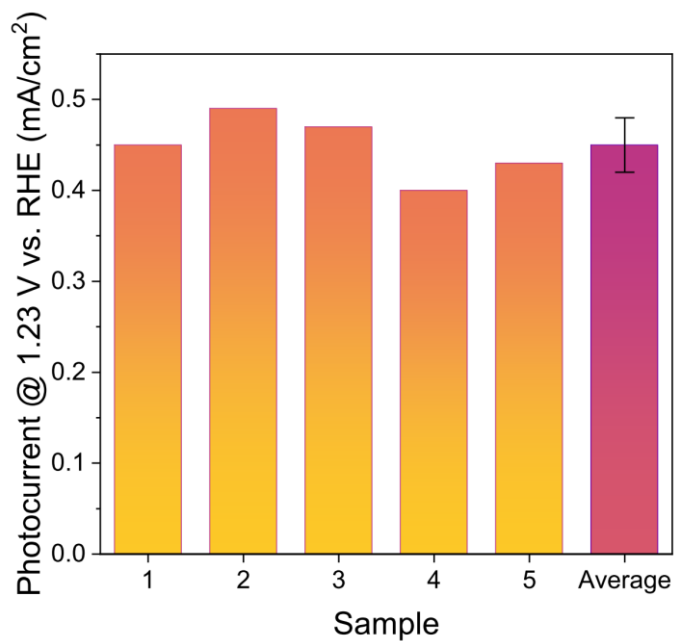


Figure S12

Chronoamperometry of a typical CuWO_4 film measured at 1.23 V vs. RHE under constant light illumination.

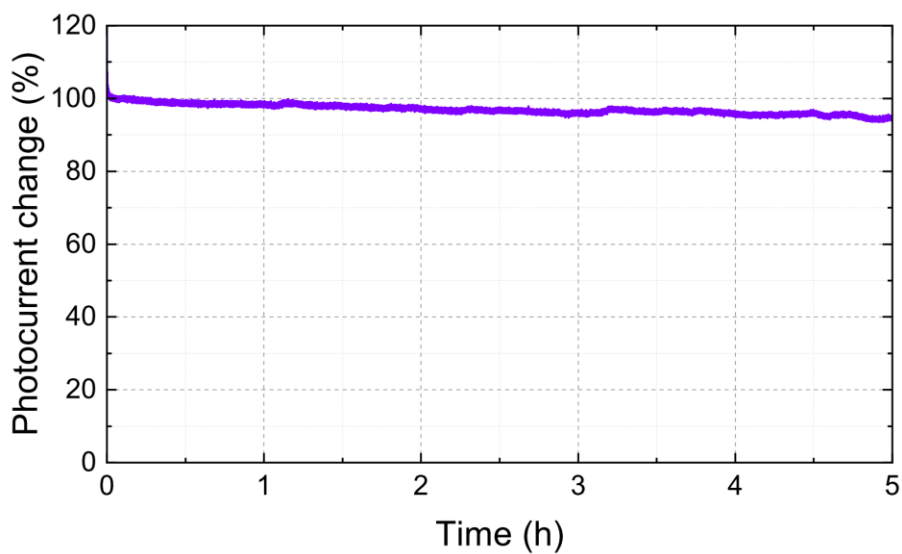


Figure S13

Extended chronoamperometry (24 hours) of a typical CuWO_4 film measured at 1.23 V vs. RHE under constant light illumination. The arrows indicate the times when the measurement was paused, and the solar simulator was checked to confirm the 1 sun intensity.

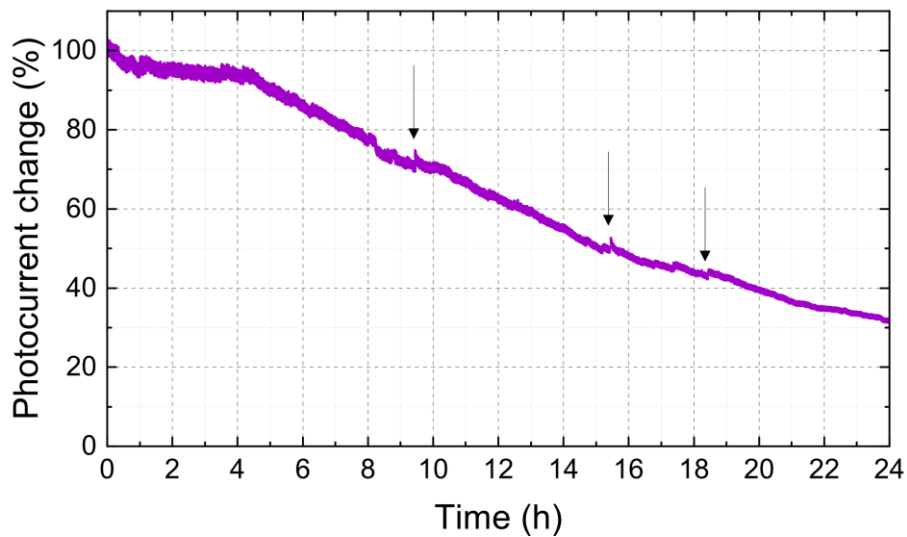


Figure S14

XPS spectra of a CuWO_4 film in the Cu 2p, W 4f and O 1s regions, before and after the 24 hours extended chronoamperometry test. No different can be detected between the spectra.

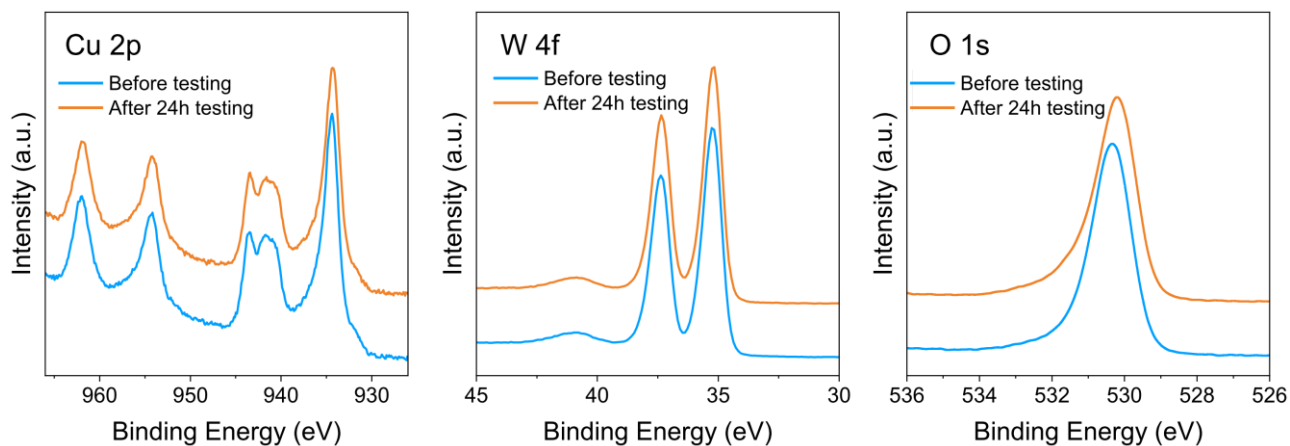


Figure S15

Raman spectra of a CuWO_4 film before and after the 24 hours extended chronoamperometry test. The arrows indicate minor peaks observed after testing, possibly due to WO_3 .

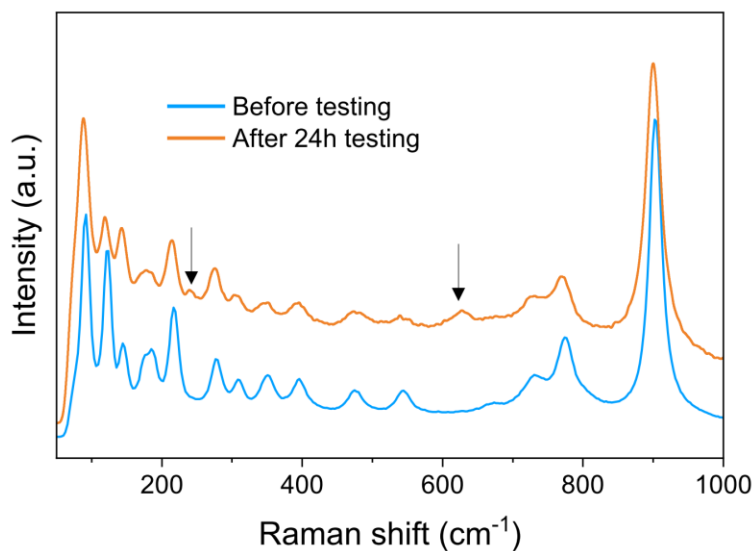


Figure S16

LSV curves for a CuWO_4 sample measured under pulsed illumination (455 nm, 25 mW/cm²). This demonstrates that the CuWO_4 synthesized here is not kinetically-limited or extraction-limited in KPi electrolyte on the timescale of the measurements. The absence of “tails” in the current when the light is turned on or off are an indication of negligible recombination and effective charge extraction, respectively.

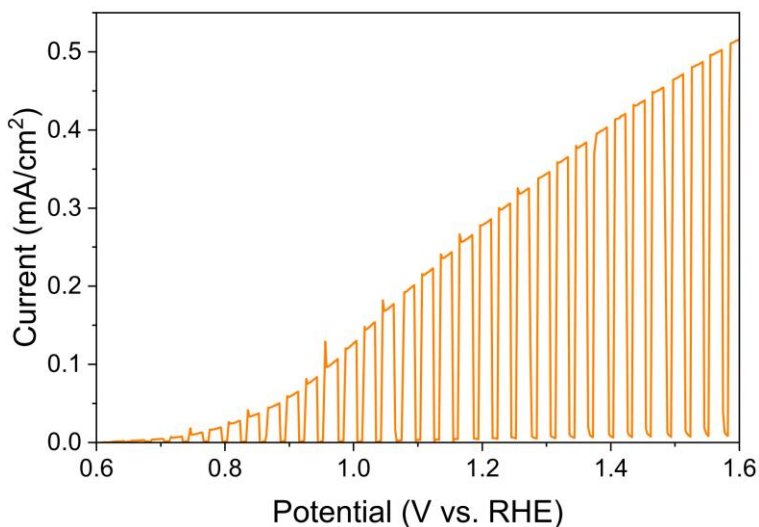


Figure S17

Optical absorption spectra for three CuWO_4 samples: standard, annealed in forming gas, and annealed in forming gas followed by the deposition of NiFeOOH co-catalysts.

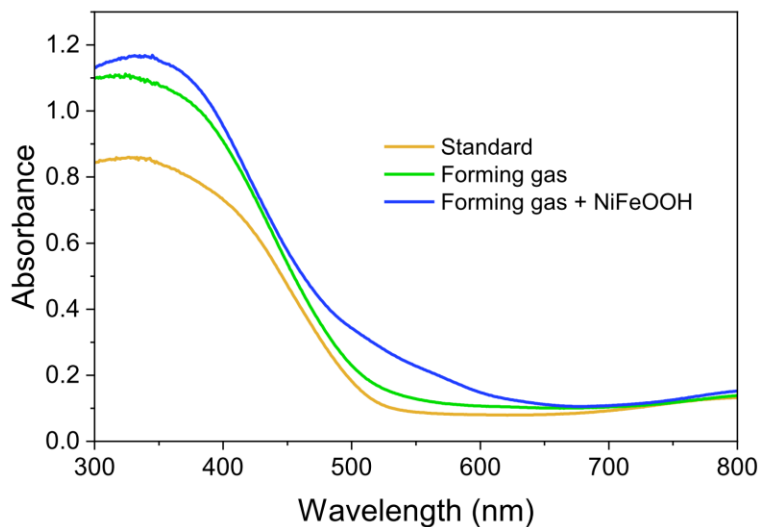


Figure S18

LSV curves measured under simulated sunlight in 0.1 M KPi with sodium sulfate as hole scavenger for three CuWO_4 samples: standard, annealed in forming gas, and annealed in forming gas followed by the deposition of NiFeOOH co-catalysts.

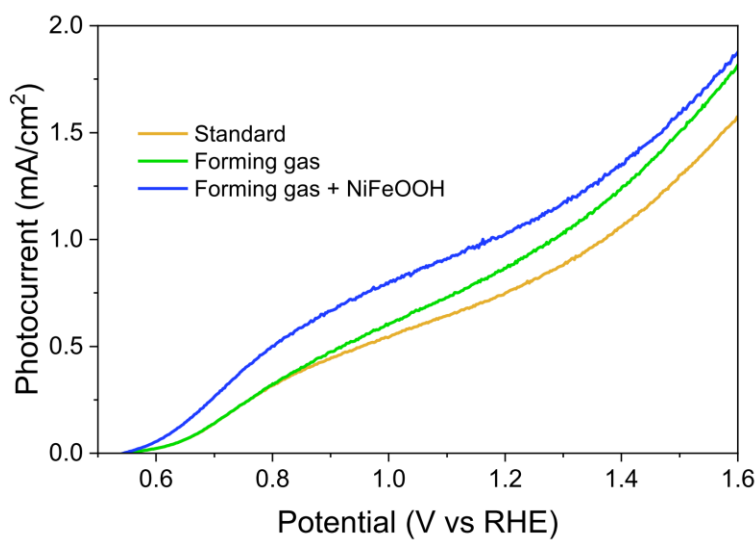


Figure S19

SEM images of CuWO_4 films (annealed at 500 °C in air), before and after further annealing at 200 °C in forming gas.

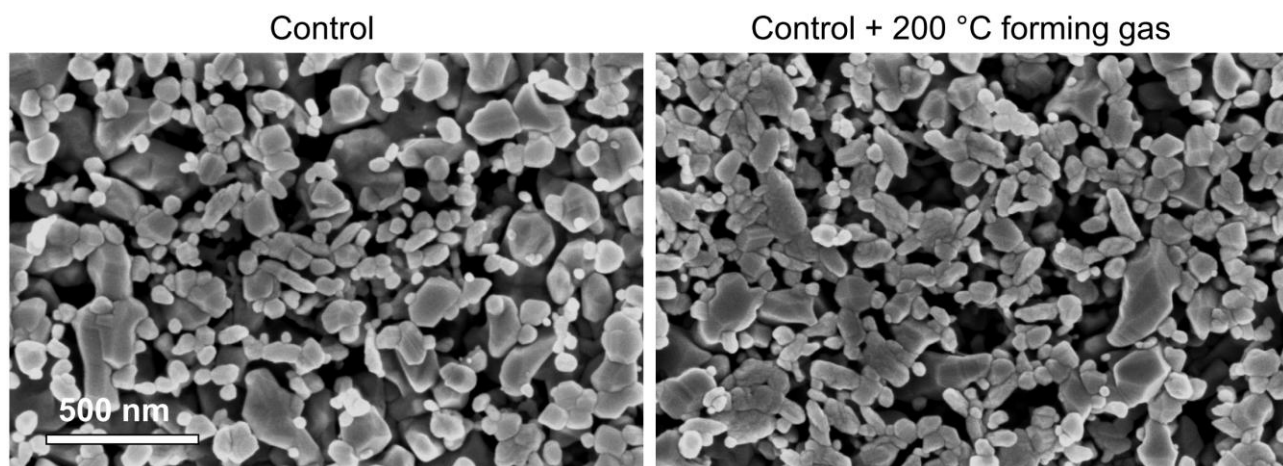


Figure S20

XRD patterns for CuWO_4 samples (previously annealed at 500 °C in air) annealed in forming gas at varying temperatures.

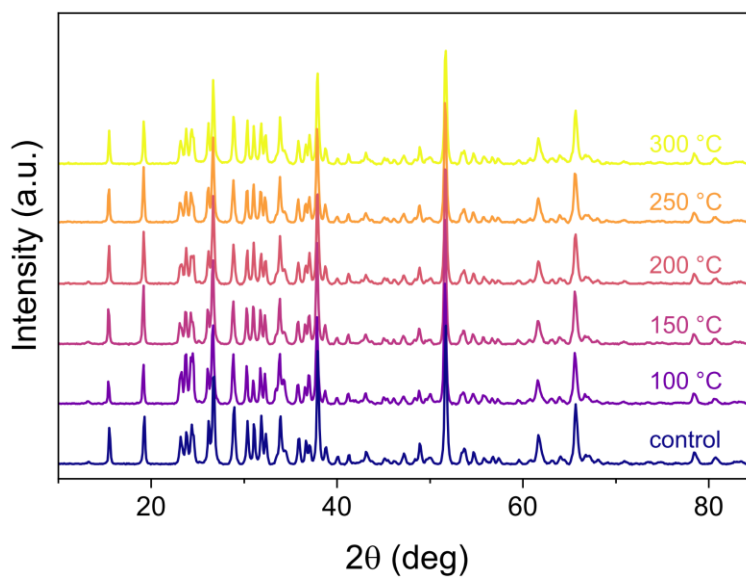


Figure S21

Optical absorption spectra for CuWO_4 samples (previously annealed at 500 °C in air) annealed in forming gas at varying temperatures.

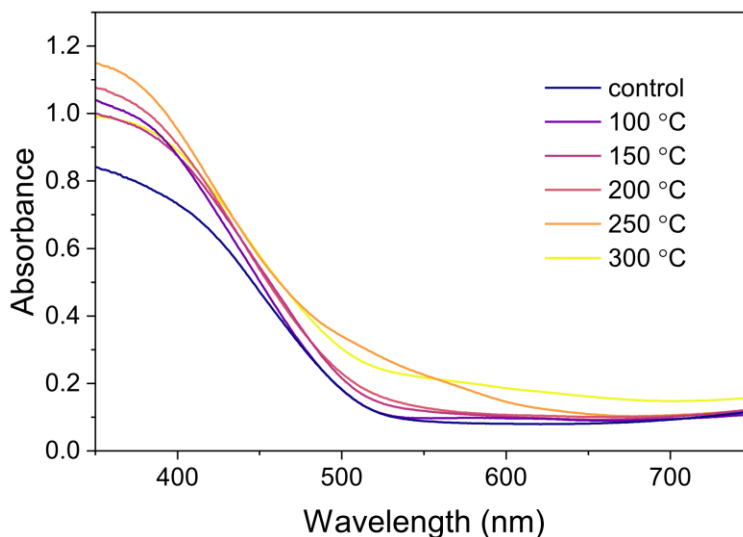


Figure S22

XPS spectra in the Cu 2p region for CuWO_4 samples (previously annealed at 500 °C in air) annealed in forming gas at varying temperatures.

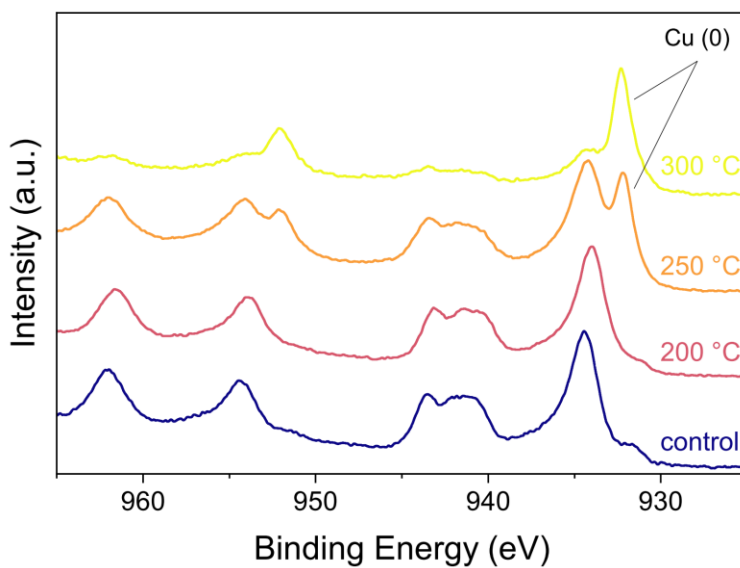


Figure S23

XPS spectra of CuWO_4 films in the Cu 2p, W 4f and O 1s regions, before and after the forming gas annealing at 200 °C.

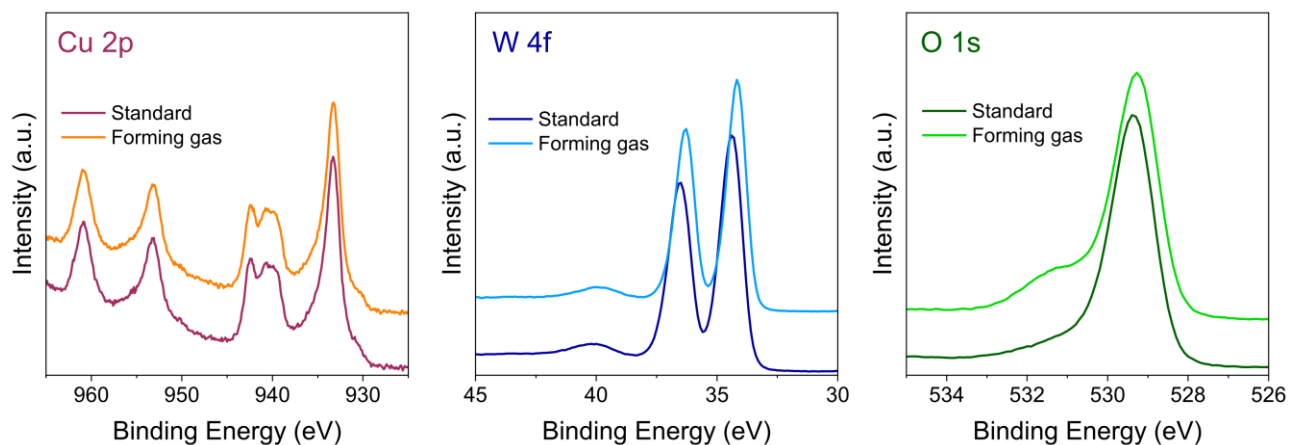


Figure S24

XPS spectra of CuWO_4 films in the Fe 2p, Ni 2p and O 1s regions, after the deposition of the NiFeOOH co-catalyst. The O 1s signal shows an additional contribution at higher binding energy ascribed to the presence of hydroxide species.

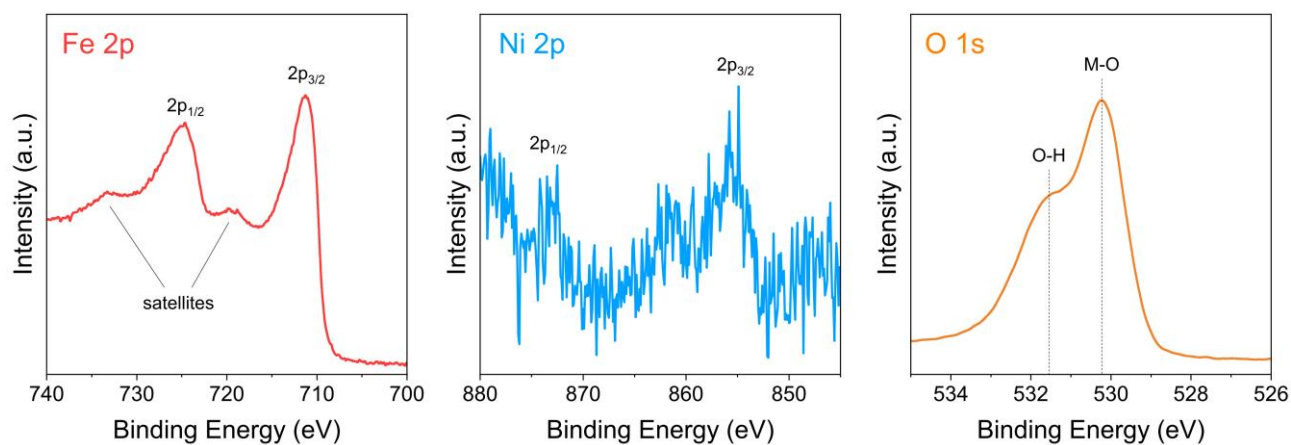
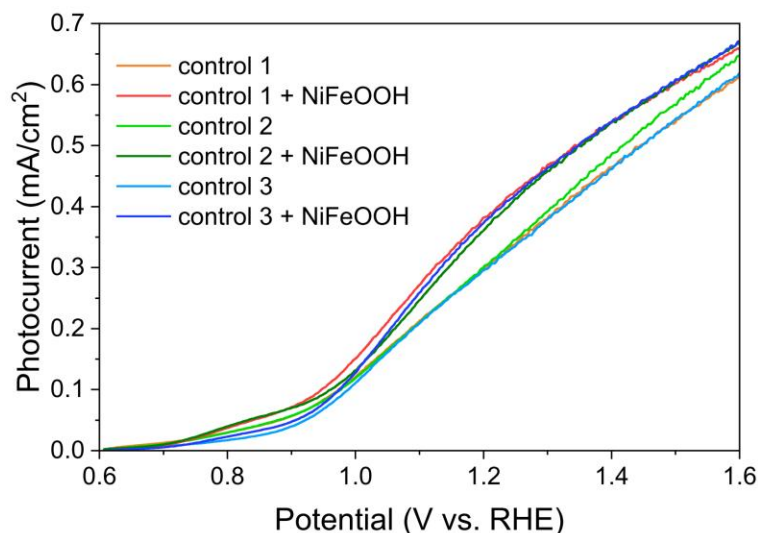


Figure S25

LSV curves under simulated sunlight for 3 nominally identical CuWO_4 samples before and after the deposition of surface co-catalysts, showing the reproducibility of the co-catalyst.



Supporting References

1. Deng, J.; Lv, X.; Zhang, H.; Zhao, B.; Sun, X.; Zhong, J., Loading the FeNiOOH cocatalyst on Pt-modified hematite nanostructures for efficient solar water oxidation. *Physical Chemistry Chemical Physics* **2016**, *18* (15), 10453-10458.
2. Pyper, K. J.; Yourey, J. E.; Bartlett, B. M., Reactivity of CuWO_4 in Photoelectrochemical Water Oxidation Is Dictated by a Midgap Electronic State. *The Journal of Physical Chemistry C* **2013**, *117* (47), 24726-24732.
3. Gao, Y.; Hamann, T. W., Elucidation of CuWO_4 Surface States During Photoelectrochemical Water Oxidation. *The Journal of Physical Chemistry Letters* **2017**, *8* (12), 2700-2704.